

The Self-Sustaining Process in Taylor-Couette Flow

Tommy Dessup, Laurette S. Tuckerman, and José Eduardo Wesfreid

Laboratoire de Physique et Mécanique des Milieux Hétérogènes (PMMH), CNRS, ESPCI Paris, PSL Research University; Sorbonne Université, Univ. Paris Diderot, France

Dwight Barkley

Mathematics Institute, University of Warwick, Coventry CV4 7AL, United Kingdom

Ashley P. Willis

School of Mathematics and Statistics, University of Sheffield, Sheffield, S3 7RH United Kingdom

(Dated: June 20, 2022)

The transition from Taylor vortex flow to wavy-vortex flow is revisited. The Self-Sustaining Process (SSP) of Waleffe [Phys. Fluids **9**, 883–900 (1997)] proposes that a key ingredient in transition to turbulence in wall-bounded shear flows is a three-step process involving rolls advecting streamwise velocity, leading to streaks which become unstable to a wavy perturbation whose nonlinear interaction with itself feeds the rolls. We investigate this process in Taylor-Couette flow. The instability of Taylor-vortex flow to wavy-vortex flow, a process which is the inspiration for the second phase of the SSP, is shown to be caused by the streaks, with the rolls playing a negligible role, as predicted by Jones [J. Fluid Mech. **157**, 135–162 (1985)] and demonstrated by Martinand et al. [Phys. Fluids **26**, 094102 (2014)]. In the third phase of the SSP, the nonlinear interaction of the waves with themselves reinforces the rolls. We show this both quantitatively and qualitatively, identifying physical regions in which this reinforcement is strongest, and also demonstrate that this nonlinear interaction depletes the streaks.

PACS numbers: 47.20.Ky, 47.20.Qr

Keywords: Taylor-Couette instability, transition to turbulence

I. INTRODUCTION

The first successful linear stability analysis for a viscous fluid was carried out in 1923 by G.I. Taylor [1] for the flow between two concentric differentially rotating cylinders. What then became known as Taylor-Couette flow has played a central role in hydrodynamic stability theory ever since. In the standard configuration of a stationary outer cylinder, as the inner cylinder rotation rate is increased, laminar flow is succeeded by axisymmetric Taylor vortices via the centrifugal instability first explained by Rayleigh [2]. The Taylor vortices subsequently develop azimuthal waves, seen in experiments by researchers such as Coles [3], Swinney and co-workers [4–6] and others [7, 8]. Wavy-vortex flow was studied computationally when this became possible in the 1980s by authors such as Jones [9, 10], Marcus [11, 12] and others [13, 14].

Taylor-Couette flow has also been studied as a way of approaching plane Couette flow, which undergoes transition to three-dimensional turbulence despite being linearly stable at all Reynolds numbers. The azimuthal, radial, and axial directions of Taylor-Couette flow play the role of the streamwise, cross-channel, and spanwise direction, respectively. As the ratio between the cylinder radii approaches one, the correspondence between the two flows becomes exact. The possibility of approaching plane Couette flow via Taylor-Couette flow has been used by many authors for many different purposes. Nagata [15] used homotopy to calculate otherwise inaccessible unstable steady states of plane Couette flow. Hristova et al. [16] and Meseguer et al. [17] compared transient growth rates between the two flows. Prigent et al. [18] extended the observation of coexisting turbulent and laminar regions seen in Taylor-Couette by Coles [3] to plane Couette flow. Faisst and Eckhardt [19] used Taylor-Couette flow to approach the turbulent lifetimes and intermittency of plane Couette flow. A very narrow gap Taylor-Couette geometry was used as a proxy for plane Couette flow by Shi et al. [20] to calculate the statistical threshold of sustained turbulence and by Lemoult et al. [21] to establish that this transition was manifested as a directed percolation phase transition.

Here, we take the analogy in the opposite direction: extending an idea developed for plane Couette flow to Taylor-Couette flow. Waleffe [22, 23] has proposed a now widely-accepted three-part mechanism, by which streamwise rolls (damped in the plane Couette case), cause streamwise streaks (by simple advection of the streamwise velocity contours), which become wavy (through instability), acquiring streamwise dependence. The nonlinear self-interaction of the wavy streaks drives the streamwise rolls, thus closing the cycle. The mechanism is similar to that proposed by Hall and co-workers [24–26] and by Beaume and co-workers [27–29]. Although the SSP was influenced by these

phenomena in Taylor-Couette flow, it has not actually not been applied to Taylor-Couette flow itself. The main purpose of this paper is to see how the Self-Sustaining Process plays out in Taylor-Couette flow, where the analogous structures, i.e. axisymmetric and wavy Taylor vortices, are actually stable equilibrium states.

II. EQUATIONS, METHODS AND PARAMETERS

The equations governing Taylor-Couette flow and the methods for computing it are sufficiently well known as to warrant only a very brief exposition. The inner and outer cylinders have radii and angular velocities R_j and Ω_j . From these, along with the kinematic viscosity ν , can be constructed the length scale $d \equiv R_2 - R_1$, the time scale d^2/ν , the two Reynolds numbers $Re_j \equiv R_j \Omega_j d/\nu$, and the radius ratio $\eta \equiv R_1/R_2$. The non-dimensionalized governing equations and boundary conditions are then

$$\partial_t \mathbf{U} = \mathbf{U} \times \nabla \times \mathbf{U} - \nabla P + \nabla^2 \mathbf{U} \quad (1a)$$

$$\nabla \cdot \mathbf{U} = 0 \quad (1b)$$

$$\mathbf{U} = Re_j \mathbf{e}_\theta \text{ at } r = r_j \equiv R_j/d, \quad j = 1, 2 \quad (1c)$$

We will restrict our consideration to the classic inner-cylinder-rotation case with $\Omega_2 = 0$ so that $Re_2 = 0$ and hence we use Re to denote the inner Reynolds number Re_1 . Nonlinear Taylor-vortex and wavy-vortex flows, denoted by TVF and WVF or \mathbf{U}_{TVF} and \mathbf{U}_{WVF} , are calculated by solving the evolution equations (1) numerically. For linear stability analysis, the nonlinear code has been adapting to solve the linearized equations

$$\partial_t \mathbf{u} = \mathbf{U} \times \nabla \times \mathbf{u} + \mathbf{u} \times \nabla \times \mathbf{U} - \nabla p + \nabla^2 \mathbf{u} \quad (2a)$$

$$\nabla \cdot \mathbf{u} = 0 \quad (2b)$$

$$\mathbf{u} = 0 \quad \text{at } r = r_j, \quad j = 1, 2 \quad (2c)$$

where \mathbf{U} is the flow whose stability is sought. Temporal integration of (2) effectively carries out the power method, converging to the eigenvector whose eigenvalue has largest real part. Most commonly, we take \mathbf{U} to be Taylor-vortex flow, \mathbf{U}_{TVF} , and the power method returns the wavy vortex eigenvector \mathbf{u}_{wvf} and corresponding eigenvalue.

The pseudospectral code we use represents functions on a spatial Chebyshev grid in the radial direction r and on equally spaced points in the azimuthal θ and axial z directions, with spatial derivatives taken via finite differences in r and by differentiation of Fourier series in θ, z . Taylor-vortex flow is calculated in an axisymmetric domain with $N_r = 33$ radial points and $N_z = 16$ points over the axial domain $[0, L_z)$ or, equivalently, multiples of the wavenumber $2\pi/L_z$. Computations of wavy-vortex flow eigenvectors use a single azimuthal mode M_0 . Nonlinear wavy-vortex flow is calculated using $N_\theta = 16$ points in the azimuthal sector $[0, 2\pi/M_0]$ or, equivalently, multiples of the wavenumber M_0 .

One difficulty is deciding which of the many TVFs or WVFs to study. Each TVF is characterized by an axial wavenumber, and each WVF has an axial and an azimuthal wavenumber. States with different wavenumbers can be simultaneously stable, as emphasized by Coles [3] and by many subsequent researchers [4, 5, 7]. Jones [10] and Antonijoan & Sanchez [14] have shown the complexity of the bifurcations and ranges of existence of wavy-vortex states with different azimuthal wavenumbers as the radius ratio and the axial wavelength are varied. We select the radius ratio to be $\eta = 0.92$, corresponding to $r_1 = 11.5$ and $r_2 = 12.5$. To make connection with the SSP in plane Couette flow, we take the axial wavelength to be $L_z = 2$, corresponding to a spanwise wavelength of 4 half-gaps as considered by Waleffe [22, 23]. (Note that the length scale in the Taylor-Couette problem is the full gap.) To approximate the streamwise wavelength of 10 half-gaps studied by Waleffe, we first express the circumferential wavelength of a wavy-vortex state with azimuthal wavenumber M_0 at the midgap $r = \bar{r}$ in units of the gap

$$L_\theta = \frac{2\pi\bar{r}}{M_0} = \frac{2\pi}{M_0} \frac{(r_2 + r_1)/2}{r_2 - r_1} = \frac{\pi}{M_0} \frac{1 + \frac{r_1}{r_2}}{1 - \frac{r_1}{r_2}} = \frac{\pi}{M_0} \frac{1 + \eta}{1 - \eta} \quad (3)$$

We use the phrase circumferential wavelength to denote a length, in contrast with an azimuthal wavelength, which is expressed in radians and necessarily a fraction of 2π . Setting $\eta = 0.92$ and $L_\theta = 5$, corresponding to 10 in half-gaps, leads to

$$M_0 = \frac{\pi}{L_\theta} \frac{1 + \eta}{1 - \eta} = \frac{\pi}{5} \frac{1.92}{0.08} \approx 15 \quad (4)$$

The critical Reynolds number for onset of Taylor-vortex flow in which only the inner cylinder rotates is approximately

$$Re_{\text{TVF}} \approx \sqrt{\frac{1708}{\eta(1-\eta)}} \frac{1+\eta}{2} \quad (5)$$

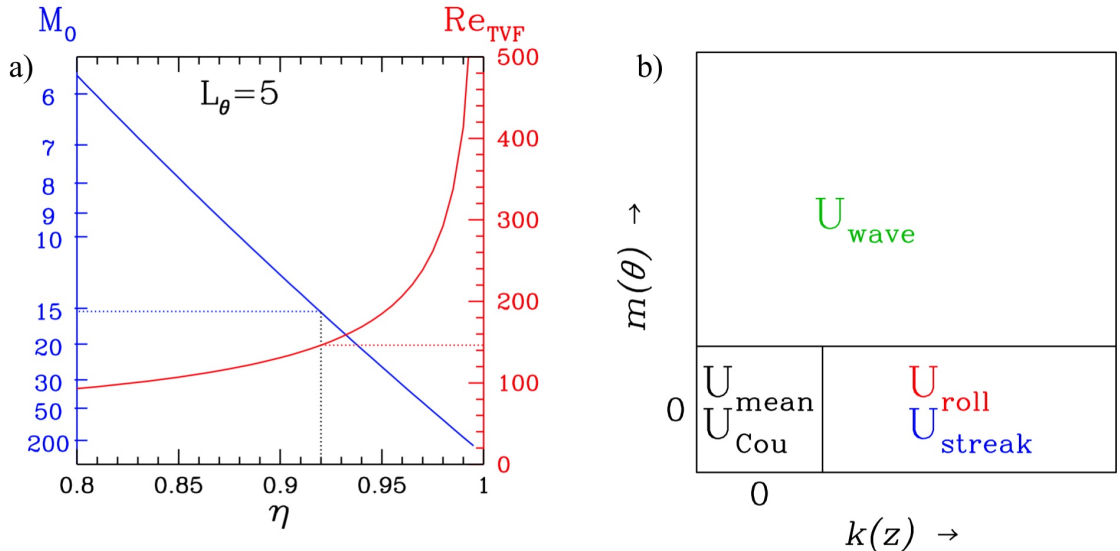


FIG. 1: (a) Dependence of critical Reynolds number Re_{TV}^{TVF} on the radius ratio η for transition to Taylor-vortex flow (right scale). Also shown is the relationship between azimuthal wavenumber M_0 and η for circumferential wavelength $L_\theta = 5$ (left scale). Our chosen parameter values are $\eta = 0.92$ and $M_0 = 15$. (b) Schematic decomposition of flow into U_{Cou} , U_{mean} , U_{roll} , U_{streak} , U_{wave} according to axial and azimuthal Fourier modes k and m .

which diverges as the narrow-gap (or plane Couette) limit $\eta \rightarrow 1$ is approached. The dependence of the critical Reynolds on η is shown in Fig. 1(a), together with the relationship between M_0 and η for $L_\theta = 5$. For $\eta = 0.92$, Taylor vortices appear above $Re_{TV}^{TVF} \approx 146$. For these values of η , L_z , and M_0 , Taylor-vortex flow remains stable until $Re_{WVF} \approx 201$, above which the flow becomes unstable to wavy Taylor vortices. Figure 2(a) shows the Taylor-vortex flow while Fig. 3 shows the wavy-vortex flow, both computed at $Re = 300$.

III. ANALYSIS IN TERMS OF SELF-SUSTAINING PROCESS

We begin our analysis by introducing notation. Flow fields \mathbf{U} can be decomposed as follows; see Fig. 1(b).

$$\mathbf{U} = \sum_k \sum_m \left(\hat{U}_r^{k,m}(r) \mathbf{e}_r + \hat{U}_\theta^{k,m}(r) \mathbf{e}_\theta + \hat{U}_z^{k,m}(r) \mathbf{e}_z \right) e^{i(kz/L_z + m M_0 \theta)} \quad (6a)$$

$$= \mathbf{U}_{Cou} + \mathbf{U}_{mean} + \mathbf{U}_{roll} + \mathbf{U}_{streak} + \mathbf{U}_{wave} \quad (6b)$$

where

$$\mathbf{U}_{Cou} \equiv \left(Ar + \frac{B}{r} \right) \mathbf{e}_\theta \quad (7a)$$

$$\mathbf{U}_{mean} \equiv \hat{U}_\theta^{0,0}(r) \mathbf{e}_\theta - \mathbf{U}_{Cou} \quad (7b)$$

$$\mathbf{U}_{roll} \equiv \sum_{k \neq 0} \left(\hat{U}_r^{k,0}(r) \mathbf{e}_r + \hat{U}_z^{k,0}(r) \mathbf{e}_z \right) e^{ikz/L_z} \quad (7c)$$

$$\mathbf{U}_{streak} \equiv \sum_{k \neq 0} \hat{U}_\theta^{k,0}(r) \mathbf{e}_\theta e^{ikz/L_z} \quad (7d)$$

$$\mathbf{U}_{wave} \equiv \sum_k \sum_{m \neq 0} \hat{\mathbf{U}}^{km}(r) e^{i(kz/L_z + m M_0 \theta)} \quad (7e)$$

Note that (7b) defines \mathbf{U}_{mean} to be the (θ, z) -independent deviation from laminar Couette flow, in contrast to Waleffe [22, 23], whose mode M includes the laminar flow (7a). In terms of this decomposition, Taylor-vortex flow

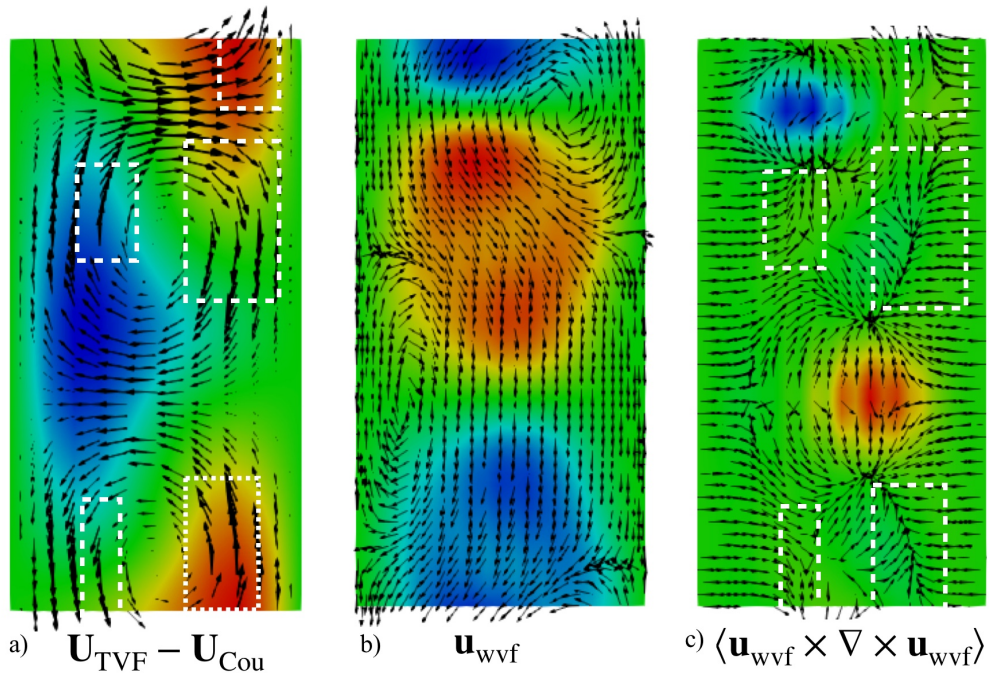


FIG. 2: Visualizations in the meridional (r, z) plane of (a) Taylor-vortex flow (without laminar Couette flow), (b) the $M_0 = 15$ eigenvector leading to wavy-vortex flow, and (c) nonlinear interaction of this eigenvector with itself. The parameters are $Re = 300$ and $\eta = 0.92$. In each case, the meridional velocity within the plane is indicated by arrows and the azimuthal velocity perpendicular to it is indicated by colors. Thus, in (a) the arrows show the rolls and the colors show the streaks of Taylor-vortex flow. The white dashed boxes in (c) and (a) highlight the resemblance between the meridional components (arrows) of $\langle \mathbf{u}_{wvf} \times \nabla \times \mathbf{u}_{wvf} \rangle$ and of the rolls of \mathbf{U}_{TVF} , which comprise the third step of the SSP.

and wavy-vortex flow take the form

$$\mathbf{U}_{TVF} = \mathbf{U}_{Cou} + \mathbf{U}_{mean} + \mathbf{U}_{roll} + \mathbf{U}_{streak} \quad (8a)$$

$$\mathbf{U}_{WVF} = \mathbf{U}_{Cou} + \mathbf{U}_{mean} + \mathbf{U}_{roll} + \mathbf{U}_{streak} + \mathbf{U}_{wave} \quad (8b)$$

Waleffe's Self-Sustaining Process [22, 23] describes three steps involving the three components \mathbf{U}_{roll} , \mathbf{U}_{streak} , and \mathbf{U}_{wave} :

A) $\mathbf{U}_{roll} \implies \mathbf{U}_{streak}$. This is a statement of kinematic advection.

B) $\mathbf{U}_{streak} \implies \mathbf{U}_{wave}$. This is described by Waleffe as a linear instability

C) $\mathbf{U}_{wave} \implies \mathbf{U}_{roll}$. The nonlinear interaction of the wave with itself creates or reinforces the rolls.

A. Rolls to streaks

The SSP begins with streamwise invariant rolls \mathbf{U}_{roll} and considers the development of streaks from these rolls. In plane Couette flow, or Waleffe's free-slip version [23] now sometimes called Waleffe flow [27–31], rolls are not themselves an equilibrium state. Hence in the planar case it is necessary to begin the SSP by inserting rolls into the flow and observing the resulting streak development. Permanent rolls and streaks have been produced in variants of plane Couette flow by including a spanwise-oriented wire or ribbon experimentally [32–34] or numerically [35]. For the Taylor-Couette problem, however, this phase is straightforward. The rolls and the streaks that they generate are contained in Taylor-vortex flow, which bifurcates supercritically and exists as a stable nonlinear equilibrium. In Fig. 2(a), calculated at $Re = 300$, the rolls are the meridional-plane flow indicated by arrows. The streaks are the axial variation in the azimuthal flow driven by the rolls and are seen as the colored patches.

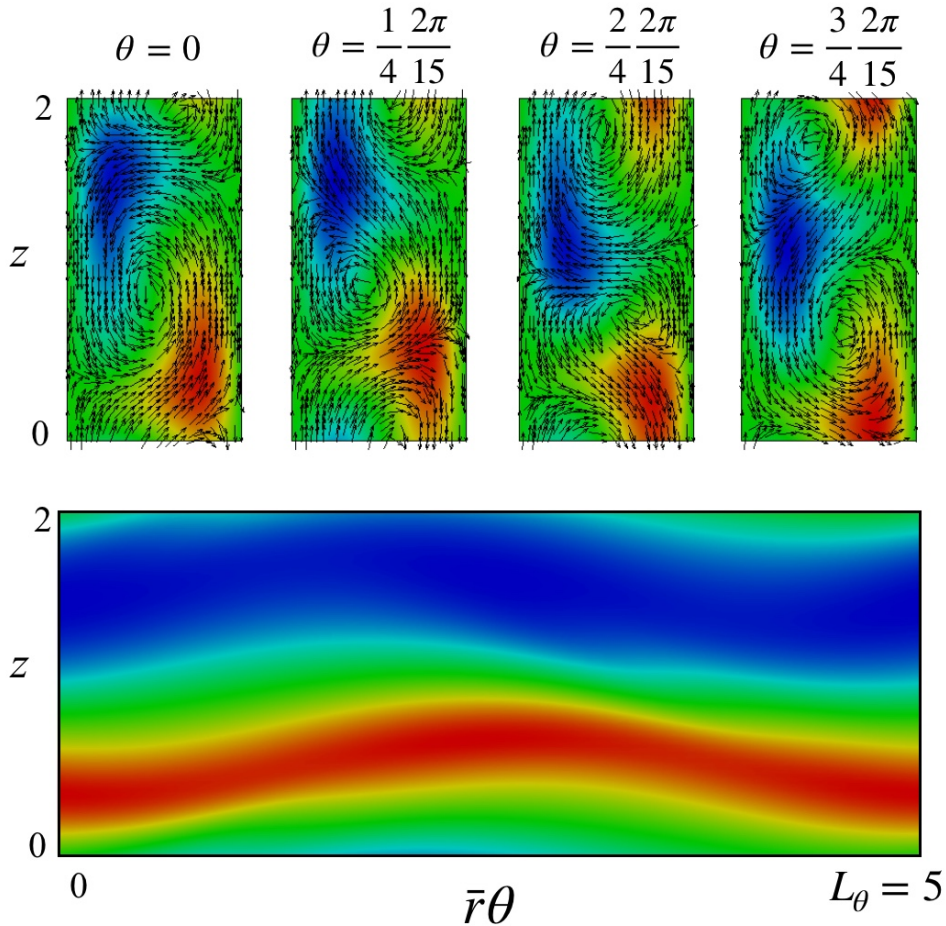


FIG. 3: Wavy-vortex flow (including Taylor-vortex flow but not laminar Couette flow) at $Re = 300$. Above: four meridional planes over azimuthal period $[0, 2\pi/15]$. Azimuthal velocity indicated by colors, meridional velocity by arrows. Below: one azimuthal period $[0, 2\pi/15]$ at mid-gap $\bar{r} = 12$. Radial velocity indicated by colors.

B. Streaks to waves

We now turn to the second stage of the SSP in which the streaks become unstable to waviness. Once again, the situation in the Taylor-Couette problem is much more clear cut in the planar case. The onset of waviness is a distinct supercritical instability – the transition from Taylor-vortex flow \mathbf{U}_{TVF} to wavy-vortex flow \mathbf{U}_{WVF} . In the \mathbf{U}_{WVF} state shown in Fig. 3, the flow has azimuthal variation (waviness) and is an azimuthally travelling wave. In 1985, Jones [10] suggested that the instability arose from the streaks, i.e. the axial variation of the azimuthal flow, which he called azimuthal jets. Thirty years later, Martinand, Serre and Lueptow [36] confirmed this idea by constructing the linear operator governing the wavy instability and showing that the eigenvalues of the portion of the operator arising from the azimuthal shear, i.e. the streaks, best matched the eigenvalues of the entire operator. They also demonstrated a number of common features between the transition to wavy vortex flow and the Kelvin-Helmholtz instability, notably a phase speed intermediate between that of the two cylinders and the multiplicity of possible azimuthal wavenumbers.

We show this by a different procedure, carrying out linearization about \mathbf{U}_{TVF} and about $\mathbf{U}_{\text{TVF}} - \mathbf{U}_{\text{roll}}$, i.e. the Taylor vortex flow without its radial or axial components. Fig. 4 compares the eigenvectors and growth rates resulting from these two linearizations. Since omitting \mathbf{U}_{roll} from the base flow barely changes the eigenvector or eigenvalue, it is clear that it plays no role in the instability. In contrast, linearization about $\mathbf{U}_{\text{TVF}} - \mathbf{U}_{\text{streak}}$, i.e. omitting the axial dependence of the azimuthal flow, leads to eigenvalues with very small growth rate and eigenvectors with no resemblance to those of \mathbf{U}_{TVF} . (These results are not displayed.) These numerical experiments confirm that the instability mechanism responsible for the transition of \mathbf{U}_{TVF} to \mathbf{U}_{WVF} is the axial variation of the azimuthal velocity.

In addition to linearization, we examine the energy content in the flow components of the nonlinear states. We decompose both Taylor-vortex flow \mathbf{U}_{TVF} and the wavy-vortex flow \mathbf{U}_{WVF} into components given in Eqs. (6)-(8)

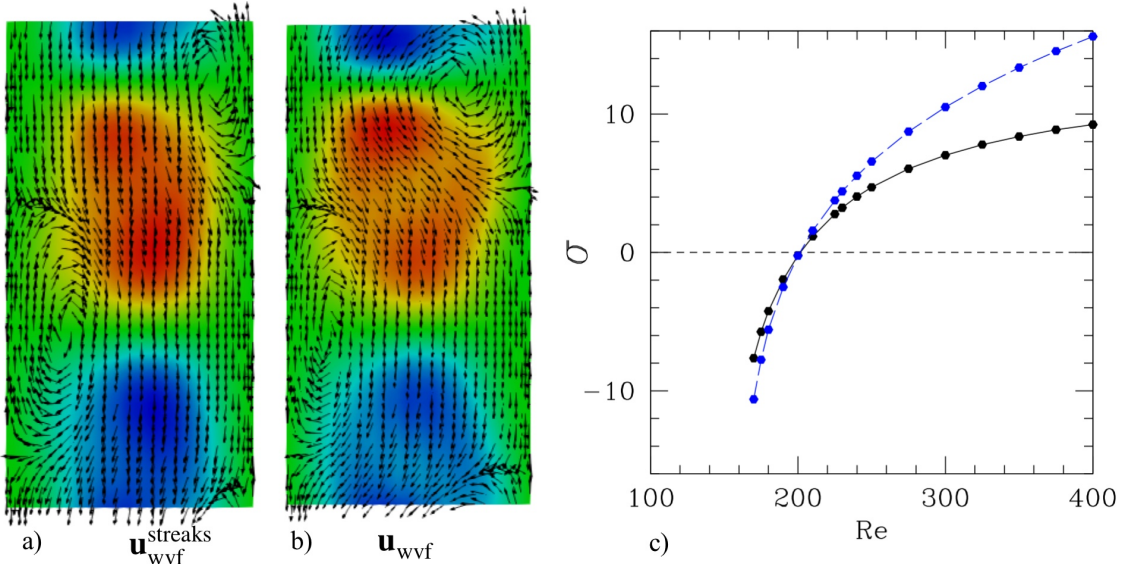


FIG. 4: Comparison of linearization about \mathbf{U}_{TVF} and about $\mathbf{U}_{\text{streak}}$. Eigenvectors resulting from linearization about (a) the full \mathbf{U}_{TVF} and (b) only $\mathbf{U}_{\text{streaks}}$ for $Re = 300$. (c) Growth rate (real part of eigenvalue) for linearization about \mathbf{U}_{TVF} (black, solid), $\mathbf{U}_{\text{streak}}$ (blue, dashed), as a function of Re .

and compute the energy of each. Fig. 5(a) shows the variation of the energy components as a function of Reynolds number. (The much larger energy of \mathbf{U}_{Cou} and a contribution combining \mathbf{U}_{Cou} and \mathbf{U}_{mean} are not shown.) \mathbf{U}_{TVF} appears at $Re = 146$ and \mathbf{U}_{WVF} appears at $Re = 201$. It can be seen that $E_{\text{streak}}^{\text{WVF}}$, the energy of the streaks in \mathbf{U}_{WVF} , is substantially decreased from the analogous quantity $E_{\text{streak}}^{\text{TVF}}$ in \mathbf{U}_{TVF} . This decrease is almost exactly counterbalanced by the energy in the waviness, $E_{\text{wave}}^{\text{WVF}}$, suggesting that the energy in the waviness is extracted from the streaks. The energy in the rolls is small and is almost the same in the two states. Thus, in addition to the linear instability mechanism, the comparison between the energy content of the saturated nonlinear states with and without waves shows that streaks feed the waves. As stated by Waleffe [23], it is not the rolls but the streaks whose energy is drained by the waves.

C. Waves to rolls

The key novelty of the SSP is the positive feedback of the waviness on the rolls. To study this in Taylor-Couette flow, we calculate the eigenvector \mathbf{u}_{wvf} responsible for the bifurcation to wavy vortices, shown in Fig. 2(b). (This complex eigenvector is shown here at one spatial or temporal phase.) We then compute the nonlinear interaction of \mathbf{u}_{wvf} with itself, in the form $\mathbf{u}_{\text{wvf}} \times \nabla \times \mathbf{u}_{\text{wvf}}$. Since $\mathbf{u}_{\text{wvf}} \sim e^{\pm i M_0 \theta}$, this quadratic term leads to azimuthal dependence of the form $e^{\pm 2i M_0 \theta}$ (second harmonic) and 1 (constant). We are interested in the constant contribution which has the form:

$$\text{NL} \equiv \langle \mathbf{u}_{\text{wvf}} \times \nabla \times \mathbf{u}_{\text{wvf}} \rangle \equiv \mathbf{u}_{\text{wvf}}^R \times \nabla \times \mathbf{u}_{\text{wvf}}^R + \mathbf{u}_{\text{wvf}}^I \times \nabla \times \mathbf{u}_{\text{wvf}}^I \quad (9)$$

A visualization of this vector quantity is shown in Fig. 2(c). This term feeds back on the θ -independent contributions \mathbf{U}_{roll} and $\mathbf{U}_{\text{streak}}$. On a qualitative level, one can see in Fig. 2 the feedback of this term on \mathbf{U}_{roll} . Highlighted regions emphasize the resemblance between the meridional flow (arrows) of NL and the rolls of Taylor-vortex flow. The resemblance is especially strong on curves of near-axial flow in NL converging towards saddles above and below regions of high azimuthal velocity.

A more quantitative picture of the feedback is presented in Fig. 5(b). Shown is the normalized inner product between NL and each of \mathbf{U}_{roll} , $\mathbf{U}_{\text{streak}}$ and \mathbf{U}_{mean} . It can be seen that NL has a positive overlap with \mathbf{U}_{roll} , meaning that indeed, the nonlinear interaction of \mathbf{u}_{wvf} with itself acts as a driving mechanism for rolls. NL also drives \mathbf{U}_{mean} . In contrast, NL has a negative overlap with $\mathbf{U}_{\text{streak}}$ and hence tends to suppress the streaks.

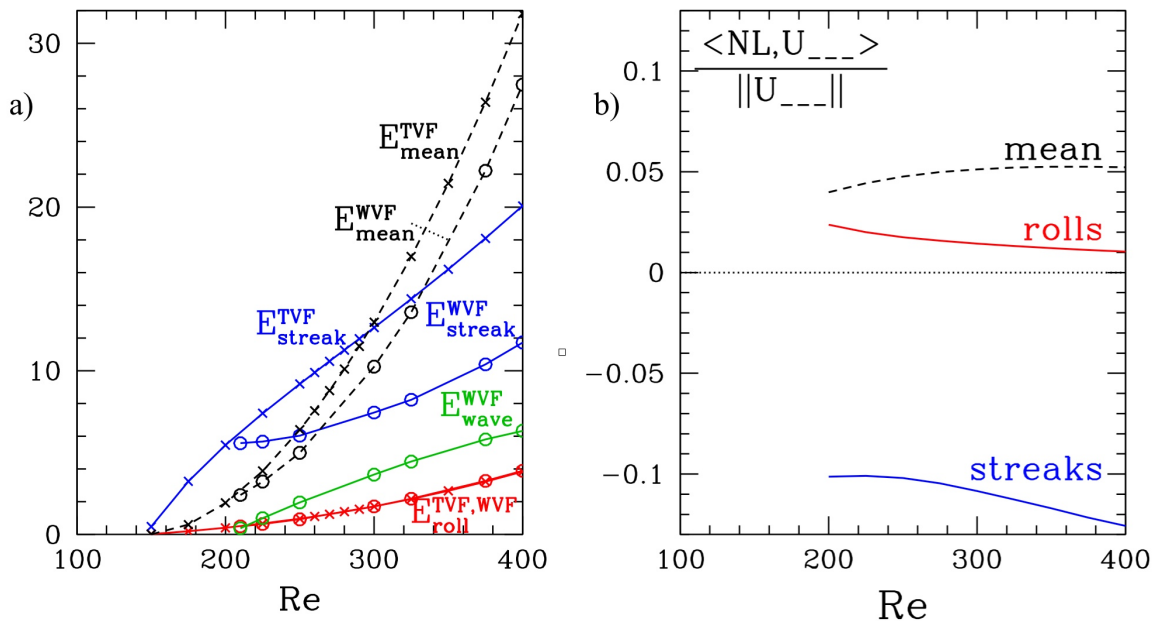


FIG. 5: (a) Energy decomposition for U_{TVF} and U_{WVF} . (See Fig. 1(b) for definitions of this decomposition.) Curves marked with crosses correspond to the components of U_{TVF} originating at $Re = 146$. Curves marked with circles correspond to the energy components of U_{WVF} which bifurcates at $Re = 201$. The streak energy is lower for WVF than it is for TVF; the difference between the two is close to the energy in the waves (which is necessarily zero for TVF). The energy in the deviation of the mean from Couette flow is also lower for WVF than for TVF. The energy in the rolls is approximately the same for the two flows. (b) Normalized inner product of nonlinear self-interaction $\langle NL, U_{rolls} \rangle / \|U_{rolls}\|$, $\langle NL, U_{streaks} \rangle / \|U_{streaks}\|$ and $\langle NL, U_{mean} \rangle / \|U_{mean}\|$ for rolls, streaks, and deviation of the mean from Couette flow. The nonlinear term NL feeds the rolls and mean and drains the streaks.

IV. CONCLUSION

According to the self-sustaining process (SSP) of [23], the building block of transition to turbulence in plane Couette flow and other wall-bounded shear flows, rolls induce streaks, which in turn undergo an instability to waviness, whose nonlinear interaction feeds the rolls. In plane Couette flow, laminar flow (the analogue of U_{Cou}) is stable for all Reynolds numbers; there is no equivalent of the steady Taylor-vortex flow. For Taylor-vortex flow, however, most of the steps of the SSP are already in place. Vortices (rolls) induce streaks (axially periodic variation of the azimuthal flow) kinematically via advection, as in plane Couette flow. We have confirmed that the instability to wavy-vortex flow is due to this variation [36]. In addition, we have shown that the energy of the waves in nonlinear wavy-vortex flow compensates almost exactly for the decreased energy in the streaks, as compared to the energy in the streaks of nonlinear Taylor-vortex flow. The third step is the feedback of the waves on the rolls, which is crucial for the SSP since in plane Couette flow the rolls do not arise from a linear instability leading to a nonlinear equilibrium. We have shown that this feedback mechanism exists in Taylor-Couette flow and that it is the rolls that are fed and not the streaks. The nonlinear self-interaction of the waves generates localized regions with strong axial forcing: this is the nature of the feedback on the Taylor vortices which closes the SSP.

-
- [1] G. Taylor, *Phil. Trans. R. Soc. Lond. A* **223**, 289 (1923).
 - [2] L. Rayleigh, *Proc. R. Soc. Lond. A* **93**, 148 (1916).
 - [3] D. Coles, *J. Fluid Mech.* **21**, 385 (1965).
 - [4] M. Gorman and H. L. Swinney, *J. Fluid Mech.* **117**, 123 (1982).
 - [5] G. P. King, Y. Li, W. Lee, H. L. Swinney, and P. S. Marcus, *J. Fluid Mech.* **141**, 365 (1984).
 - [6] C. D. Andereck, S. Liu, and H. L. Swinney, *J. Fluid Mech.* **164**, 155 (1986).
 - [7] J. Hegseth, G. Baxter, and C. Andereck, *Phys. Rev. E* **53**, 507 (1996).
 - [8] S. T. Wereley and R. M. Lueptow, *J. Fluid Mech.* **364**, 59 (1998).
 - [9] C. Jones, *J. Fluid Mech.* **102**, 249 (1981).
 - [10] C. Jones, *J. Fluid Mech.* **157**, 135 (1985).
 - [11] P. S. Marcus, *J. Fluid Mech.* **146**, 45 (1984).
 - [12] P. S. Marcus, *J. Fluid Mech.* **146**, 65 (1984).
 - [13] W. Edwards, S. Beane, and S. Varma, *Phys. Fluids* **3**, 1510 (1991).
 - [14] J. Antonijoan and J. Sanchez, *Phys. Fluids* **14**, 1661 (2002).
 - [15] M. Nagata, *J. Fluid Mech.* **217**, 519 (1990).
 - [16] H. Hristova, S. Roch, P. J. Schmid, and L. S. Tuckerman, *Phys. Fluids* **14**, 3475 (2002).
 - [17] Á. Meseguer, *Phys. Fluids* **14**, 1655 (2002).
 - [18] A. Prigent, G. Gregoire, H. Chate, O. Dauchot, and W. van Saarloos, *Phys. Rev. Lett.* **89**, 014501 (2002).
 - [19] H. Faisst and B. Eckhardt, *Phys. Rev. E* **61**, 7227 (2000).
 - [20] L. Shi, M. Avila, and B. Hof, *Phys. Rev. Lett.* **110**, 204502 (2013).
 - [21] G. Lemoult, L. Shi, K. Avila, S. V. Jalikop, M. Avila, and B. Hof, *Nature Physics* **12**, 254 (2016).
 - [22] F. Waleffe, *Stud. Appl. Math.* **95**, 319 (1995).
 - [23] F. Waleffe, *Phys. Fluids* **9**, 883 (1997).
 - [24] P. Hall and F. T. Smith, *J. Fluid Mech.* **227**, 641 (1991).
 - [25] P. Hall and S. Sherwin, *J. Fluid Mech.* **661**, 178 (2010).
 - [26] H. M. Blackburn, P. Hall, and S. J. Sherwin, *J. Fluid Mech.* **726** (2013).
 - [27] C. Beaume, E. Knobloch, G. P. Chini, and K. Julien, *Fluid Dyn. Res.* **47**, 015504 (2014).
 - [28] C. Beaume, G. P. Chini, K. Julien, and E. Knobloch, *Phys. Rev. E* **91**, 043010 (2015).
 - [29] C. Beaume, E. Knobloch, G. P. Chini, and K. Julien, *Phys. Scr.* **91**, 024003 (2016).
 - [30] M. Chantry, L. S. Tuckerman, and D. Barkley, *J. Fluid Mech.* **791** (2016).
 - [31] M. Chantry, L. S. Tuckerman, and D. Barkley, *J. Fluid Mech.* **824** (2017).
 - [32] O. Dauchot and F. Daviaud, *Phys. Fluids* **7**, 335 (1995).
 - [33] S. Bottin, O. Dauchot, and F. Daviaud, *Phys. Rev. Lett.* **79**, 4377 (1997).
 - [34] S. Bottin, O. Dauchot, F. Daviaud, and P. Manneville, *Phys. Fluids* **10**, 2597 (1998).
 - [35] D. Barkley and L. S. Tuckerman, *Phys. Fluids* **11**, 1187 (1999).
 - [36] D. Martinand, E. Serre, and R. M. Lueptow, *Phys. Fluids* **26**, 094102 (2014).